Magnetic circular x-ray dichroism in emission for disordered Co-Rh-based ternary alloys

1999 J. Phys.: Condens. Matter 11 9095

(http://iopscience.iop.org/0953-8984/11/46/311)

J. Phys.: Condens. Matter **11** (1999) 9095–9103. Printed in the UK PII: S0953-8984(99)05626-X

Magnetic circular x-ray dichroism in emission for disordered Co–Rh-based ternary alloys

S Ostanin†‡, V Popescu†, H Ebert† and H Dreyssé‡

† Institute for Physical Chemistry, University of Munich, Butenandtstrasse 5-13, D-81377 München, Germany

‡ IPCMS-GEMME, 23, rue du Loess, F-67037, Strasbourg Cédex, France

Received 30 June 1999, in final form 11 October 1999

Abstract. Fully relativistic investigations on the magnetic circular dichroism in emission have been performed for Rh in the three alloy systems $Co_{0.75}Rh_{0.25}$, $Co_{0.75-x}Rh_{0.25}Ni_x$, and $Co_{0.75}Rh_{0.25-x}Pd_x$. The results obtained using the spin-polarized relativistic Korringa–Kohn–Rostoker method of band-structure calculations together with the coherent-potential approximation (SPR-KKR-CPA) allow one to make a detailed interpretation of corresponding experimental data. The changes in the magnetic moments of Co and Rh in the binary alloy Co_xRh_{1-x} caused by substitution of Pd for Rh and Ni for Co, respectively, are discussed in comparison with experimental data and a generalized Slater–Pauling curve.

1. Introduction

During the last decade magnetic circular dichroism in x-ray absorption (MCD-XA) has been established as a new tool for investigating magnetic properties of multi-component systems in an element-specific way. Although XA probes unoccupied states above the Fermi energy, the MCD sum rules [1–4] allow one to estimate the spin and orbital magnetic moments of the absorbing atom. Among the many investigations done using MCD-XA, several studies have been performed also on 4d-transition-metal elements in binary alloys [5, 6] and multi-layer systems [7, 8] during the last few years.

In contrast to XA, the corresponding x-ray emission (XE) experiment probes directly the occupied states of a system. Unfortunately, corresponding MCD-XE experiments are much more demanding than in the case of MCD-XA. For this reason, only very little experimental work has been done in this field. In particular, the element-selective nature of MCD-XE has been exploited only recently by Gallet *et al* [9] who performed investigations on Rh in Co–Rh-based ternary alloys. In this case, resonant excitation energy just above the Rh L_3-absorption edge was used, leading to a MCD-XE spectrum that reflects the magnetization of the Rh atoms induced by the neighbouring magnetic atoms.

For Co-rich binary Co_xNi_{1-x} alloys the average magnetic moment decreases nearly linearly with increasing Ni concentration, in line with the generalized Slater–Pauling construction for two strong ferromagnets [9, 10]. Accordingly, one would expect a decrease in the average moment of Co_xRh_{1-x} alloys upon substitution of Ni for Co. However, corresponding MCD-XE investigations for Rh in the alloys $Co_{0.75}Rh_{0.25}$ and $(Co_{0.85}Ni_{0.15})_{0.75}Rh_{0.25}$ did not reflect this expected change [9]. This finding was attributed to a hybridization of Ni and Rh states near the Fermi level [9]. For a substitution of Pd atoms for Rh an increase of the average

0953-8984/99/469095+09$30.00

moment may be expected because of the higher spin susceptibility of Pd compared to Rh. This expectation was indeed confirmed by MCD-XE experiments for Rh in $Co_{0.75}Rh_{0.25}$ and $Co_{0.75}(Rh_{0.85}Pd_{0.15})_{0.25}$ [9].

The experimental work of Gallet *et al* [9] on Co–Rh-based alloys was accompanied by band-structure calculations for ordered Co_3Rh. This allowed these authors to demonstrate a qualitative correlation of the MCD-XE spectra and the difference in the theoretical spin-resolved density of occupied states [9]. To permit a more detailed discussion of the properties of Co–Rh-based alloys, corresponding band-structure calculations have been performed using the spin-polarized relativistic Korringa–Kohn–Rostoker method of band-structure calculations together with the coherent-potential approximation (SPR-KKR-CPA) which in particular accounts for the disordered state of these systems. To deal with the MCD-XE the band-structure calculations have been done in a fully relativistic way. To derive from these the corresponding spectra the absorption-followed-by-emission model of Strange and co-workers [11] has been adopted.

In the following section some technical details of our work will be sketched. The major part of this contribution will be devoted to the presentation and discussion of our results.

2. Theoretical framework

The Green's function formalism supplies an appropriate framework for dealing with the electronic structure of disordered alloys. Using multiple-scattering theory, the single-electron Green's function can be written as [12, 13]

$$G^{+}(\vec{r}'_n, \vec{r}_m, E) = \sum_{\Lambda\Lambda'} Z_{\Lambda}(\vec{r}'_n, E)\tau^{nm}_{\Lambda\Lambda'}(E)Z^{\times}_{\Lambda'}(\vec{r}_m, E) - \sum_{\Lambda} Z_{\Lambda}(\vec{r}_<, E)J^{\times}_{\Lambda}(\vec{r}_>, E)\delta_{nm}. \tag{1}$$

Working in a spin-polarized relativistic mode, the functions Z_Λ and J_Λ are the regular and irregular, respectively, solutions to the single-site Dirac equation for a spin-dependent potential. The index $\Lambda = (\kappa, \mu)$ is shorthand notation for the relativistic spin–orbit and magnetic quantum numbers [14]. The quantity $\tau^{nm}_{\Lambda\Lambda'}$ in equation (1) is the so-called scattering path operator [12] that represents all multiple-scattering processes in the solid. For disordered alloys the wave functions in equation (1) refer to a specific component α, and the scattering path operator $\tau^{nm}_{\Lambda\Lambda'}$ has to be defined and determined accordingly [12]. Using the CPA to account for disorder, the latter is done by solving iteratively the so-called CPA equations giving, in particular, the site-diagonal scattering path operator $\tau^{nn,\alpha}_{\Lambda\Lambda'}$ for the component α. With the Green's function available, self-consistent calculations can be done in a more or less straightforward way, within the framework of relativistic spin-density functional theory (SDFT).

Multiple-scattering theory is also used as a standard basis to deal with x-ray absorption. A corresponding expression for the absorption coefficient $\mu^{\vec{q}\lambda}$ is given by [15]

$$\mu^{\vec{q}\lambda}_{XA}(\omega_{in}) \propto \mathrm{Im} \sum_{i} \sum_{\mathrm{unocc}} \left[\sum_{\Lambda,\Lambda'} M^{\vec{q}\lambda,\alpha *}_{\Lambda\Lambda_i}(E)\tau^{nn,\alpha}_{\Lambda\Lambda'}(E)M^{\vec{q}\lambda,\alpha}_{\Lambda\Lambda_i}(E) - \sum_{\Lambda} I^{\vec{q}\lambda,\alpha}_{\Lambda'\Lambda_i}(E) \right] \tag{2}$$

where the sum runs over the core states i involved and the radiation field is specified by the wave vector $\vec{q}$, the energy ω, and the polarization λ. With the electron–photon interaction operator defined as $X_{\vec{q}\lambda} = -e\vec{\alpha} \cdot \vec{A}_{\vec{q}\lambda}$ [15], the matrix element $M^{\vec{q}\lambda,\alpha}_{\Lambda\Lambda_i}$ in equation (2) is given by

$$M^{\vec{q}\lambda,\alpha}_{\Lambda\Lambda_i} = \int \mathrm{d}^3 r \; Z_{\Lambda}{}^{\alpha\times}(\vec{r}, E)X_{\vec{q}\lambda}(\vec{r})\phi_{\Lambda_i}(\vec{r}, E_c) \tag{3}$$

where $\vec{\alpha}$ is the vector of the standard Dirac matrices [14], $\vec{A}_{\vec{q}\lambda}$ is the vector potential of the radiation field, and $\phi_{\Lambda_i}(\vec{r}, E_c)$ is the core wave function for core state i at energy E_c. A

corresponding expression can be given for the atomic matrix element $I^{\vec{q}\lambda,\alpha}_{\Lambda\Lambda_i}$ that is connected with the irregular solution J_Λ to the Dirac equation (see equation (1)). As indicated by the superscript α, equation (2) can straightforwardly be applied to disordered alloys with all quantities evaluated for each component individually.

Experiments on the MCD-XE are usually performed using circularly polarized light for excitation and detecting the following fluorescence radiation [16]. To allow for a theoretical and experimental description for this quite complex situation, Strange *et al* [11] suggested treating the absorption and emission processes completely independently and omitting the polarization analysis for the emitted radiation. This leads to the rather simple expression for the emission intensity

$$I^{\lambda}(\omega_{in}, \omega_{out}) \propto \frac{1}{\Gamma^2} W^{\lambda}_{XA}(\omega_{in}) \sum_{\lambda'} W^{\lambda'}_{XE}(\omega_{out}) \tag{4}$$

that depends on the frequency ω_{in} and polarization λ of the exciting radiation and the frequency ω_{out} of the outgoing fluorescence radiation. Because no polarization analysis is done for the latter, one has to sum over the various polarization states λ'. The spectral function $W^{\lambda}_{XA}(\omega_{in})$ in equation (4) is the cross section for the absorption step as given by equation (2), while $W^{\lambda'}_{XE}(\omega_{out})$ is that for the emission process, which can also be dealt with using the expression in equation (2).

Using the x-ray emission intensity defined by equation (4) one can derive the corresponding circular dichroism signal from the definition

$$\Delta I_{MCD-XE} = \frac{I^{+} - I^{-}}{I^{+} + I^{-}} \tag{5}$$

that depends on the frequencies of the incoming and outgoing radiation, ω_{in} and ω_{out}, respectively.

To allow a direct comparison of results based on equations (2) and (4), respectively, one has to account for different broadening mechanisms, as indicated by the factor $1/\Gamma^2$ in equation (4). For the x-ray absorption this has been described in detail by for example Müller *et al* [15, 17]. For the x-ray emission spectra we followed the procedure suggested by Durham *et al* [18]. This means in particular that a Lorentzian linewidth $\Gamma(E)$ has been used that depends quadratically on the energy difference $E - E_F$, with E_F being the Fermi energy, and that is meant to represent relaxation of the valence band hole states due to Auger processes.

3. Results and discussion

3.1. Band-structure calculations

The properties of normally non-magnetic transition metals dissolved substitutionally in a ferromagnetic host like Fe, Co, or Ni have been studied extensively in the past [19–22]. In particular, a rather simple explanation could be given for the orientation of the induced spin magnetic moment with respect to the host magnetization. For the late transition metals one finds a parallel alignment. Within a tight-binding model this is explained by the fact that for the dominating d electrons the atomic energy parameters ϵ_d of the impurity and the host element are rather close to one another for the majority-spin system. For the minority-spin system, these are further apart, leading to a stronger binding for the majority-spin system. This situation still holds for concentrated alloys and accordingly one finds for fcc Co_xRh_{1-x} a positive spin magnetic moment for Rh that—starting with $\mu^{spin}_{\mathrm{Rh}} = 0.486\,\mu_B$ for x approaching unity [23]—decreases monotonically with increasing Rh concentration.

For the ternary alloy systems studied here, the situation scarcely changes. This can be seen in figure 1, where the spin-resolved partial density of states (DOS) is given for $(Co_{0.85}Ni_{0.15})_{0.75}Rh_{0.25}$ and $Co_{0.75}(Rh_{0.85}Pd_{0.15})_{0.25}$. All these systems are dominated by the component Co, and show accordingly partial DOS curves that are very similar to those of pure fcc Co. Rh, on the other hand, has a broad d-band complex that is rather featureless. Only in the vicinity of the Fermi level one notes a reminiscence of the virtual bound state peak that occurs for Rh impurities in Co. As can be seen in figures 1 and 2, the induced spin polarization, i.e. the difference $n^{\uparrow}_{\mathrm{Rh}}(E)-n^{\downarrow}_{\mathrm{Rh}}(E)$ of the DOS for spin up and down, respectively, is most pronounced around the Fermi level. This is primarily because the bandwidth of the magnetic 3d-transition-metal alloy partner is quite small compared to that of Rh. For Pd in $Co_{0.75}(Rh_{0.85}Pd_{0.15})_{0.25}$ the situation is quite similar to that for Rh. The differences that can be seen in figure 1 occur primarily because the Pd concentration is lower and the Pd d band is nearly filled. Finally, for Ni in $(Co_{0.85}Ni_{0.15})_{0.75}Rh_{0.25}$ the DOS is dominated by a narrow d-band complex that shows an appreciable exchange splitting.

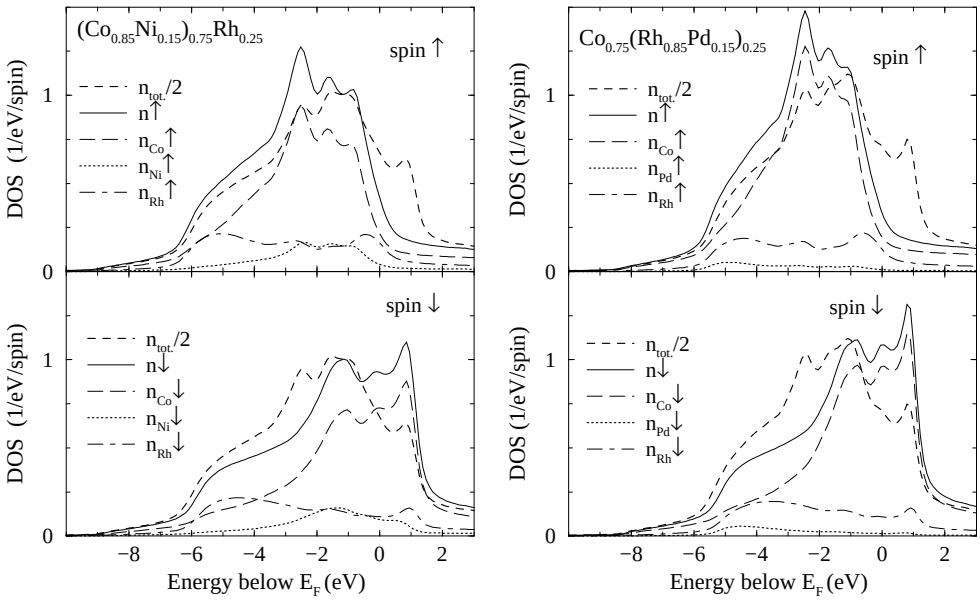

Figure 1. Component- and spin-resolved density-of-states curves for (left) $(Co_{0.85}Ni_{0.15})_{0.75}Rh_{0.25}$ and (right) $Co_{0.75}(Rh_{0.85}Pd_{0.15})_{0.25}$ alloys. The upper and lower panels give the results for the majority- and minority-spin systems, respectively. The component-resolved curves $n^{m_s}_{\alpha}(E)$ (α = Co, Rh, Ni, Pd; $m_s = \uparrow, \downarrow$) are weighted by the corresponding concentrations. For comparison the total density of states $n(E)$ is given in all panels multiplied by a factor of 0.5.

The spin magnetic moments for the various systems studied are given in table 1. For the binary alloy system Co_xRh_{1-x} the spin magnetic moment μ^{spin} of Co increases monotonically with decreasing Co concentration x [23]. This increase, that can be seen in table 1 for the specific concentration $x = 0.75$, is compensated by the much smaller moment of Rh leading to a decrease of the average moment $\bar{\mu}^{spin}$ compared to that for pure fcc Co. As was predicted before on the basis of the Slater–Pauling curve [24], partial substitution for Co in $Co_{0.75}Rh_{0.25}$ with Ni leads indeed to a reduction of $\bar{\mu}^{spin}$. While the moment μ^{spin} of Co is hardly affected by this, μ^{spin} for Rh is reduced by 15%. Nevertheless, the reduction of the total spin magnetic moment $\bar{\mu}^{spin}$ stems primarily from the spin magnetic moment of Ni, which is much smaller than μ^{spin}_{Co}. Here one should note that μ^{spin}_{Ni} for Ni in $(Co_{0.85}Ni_{0.15})_{0.75}Rh_{0.25}$ is increased by

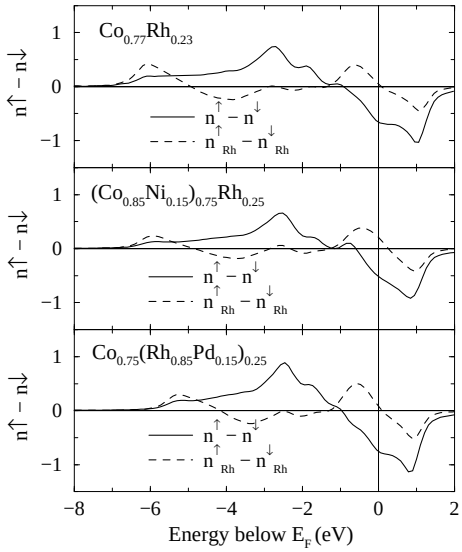

Figure 2. The differences of the spin-up and spin-down DOS $n^{\uparrow}(E) - n^{\downarrow}(E)$ for $Co_{0.75}Rh_{0.25}$-based alloys. In each part, the full line gives the average for the alloy system while the dashed line gives the results for Rh.

Table 1. The spin (μ^{spin}) and orbital (μ^{orb}) magnetic moments in Co–Rh-based alloys (in μ_B).

		μ^{spin}	μ^{orb}
$Co_{0.75}Rh_{0.25}$	Co	1.684	0.081
	Rh	0.434	0.012
	Total	1.384	0.066
$(Co_{0.85}Ni_{0.15})_{0.75}Rh_{0.25}$	Co	1.690	0.085
	Rh	0.369	0.012
	Ni	0.689	0.048
	Total	1.247	0.063
$Co_{0.75}(Rh_{0.85}Pd_{0.15})_{0.25}$	Co	1.801	0.105
	Rh	0.498	0.026
	Pd	0.244	0.021
	Total	1.465	0.085

about 15% compared to that for pure fcc Ni. This means that as regards Co and Ni the findings for $(Co_{0.85}Ni_{0.15})_{0.75}Rh_{0.25}$ are completely in line with the properties of the binary alloy system Co_xNi_{1-x}.

Partly substituting for Rh in $Co_{0.75}Rh_{0.25}$ with Pd has quite complex consequences. First of all, one notes that μ^{spin}_{Co} increased more compared to that for pure fcc Co than in the case of $Co_{0.75}Rh_{0.25}$. This is in line with the results for the binary alloy system Co_xPd_{1-x} [23]. For Pd, the induced spin magnetic moment in $Co_{0.75}(Rh_{0.85}Pd_{0.15})_{0.25}$ is smaller than for Rh. This could be expected from the properties of these two 4d transition metals. When Pd is dissolved substitutionally in fcc Co, μ^{spin}_{Pd} is found to be 0.238 μ_B, while for Rh one has $\mu^{spin}_{Rh} = 0.486\ \mu_B$ [23]. These theoretical results obtained using the single-site approximation are in reasonable agreement with results obtained by Stepanyuk *et al* [19] (0.29 μ_B for Pd and 0.5 μ_B for Rh) who accounted in addition for the distortion of the neighbouring Co-host atoms.

Finally, one notes in table 1 an increase by nearly 20% for μ_{Rh}^{spin} in $Co_{0.75}(Rh_{0.85}Pd_{0.15})_{0.25}$ compared to $Co_{0.75}Rh_{0.25}$. Presumably this is caused by the increase of μ_{Co}^{spin}.

Because our calculations have been performed on a fully relativistic level they give directly access to the spin–orbit-induced orbital magnetic moment μ^{orb}. The corresponding results have been included in table 1. As one can see, these supply contributions up to 10% to the various partial magnetic moments. Here one should note that our calculations have been done in the framework of plain spin-density functional theory (SDFT) which often gives an orbital magnetic moment that is too small. For pure Co for example the deviation from experiment amounts to about 46% while for pure Ni it can be neglected [25]. For the 4d elements only the minor corrections for μ^{orb} given in table 1 are to be expected, when one is going beyond the SDFT level, for example by including Brooks's orbital polarization (OP) scheme [26].

Starting from a spin-polarized band-structure calculation and treating spin–orbit coupling as a perturbation represented by the simplified operator $\mathcal{H}_{SOC} = \xi l_z \sigma_z$, a rather simple expression can be given for the spin–orbit-induced orbital magnetic moment. In particular, one finds that for transition metals μ_α^{orb} is given essentially by the spin polarization of the d electrons at the Fermi energy: $n_\alpha^{d\uparrow}(E_F) - n_\alpha^{d\downarrow}(E_F)$ [21]. For 3d- and 4d-transition-metal impurities at the (001) surface of Fe a semi-quantitative agreement could be found for results obtained from this simple model and the properly calculated moments μ_α^{orb}.

3.2. Magnetic circular dichroism in x-ray emission

As mentioned above, the MCD-XA can be used to derive, on the basis of the sum rules, from experimental x-ray absorption spectra an estimate of the spin and orbital magnetic moments of the absorbing atom. Corresponding work on Rh in binary Co_xRh_{1-x} alloys has been done by Harp *et al* [5, 27] who made measurements at the $M_{2,3}$ absorption edges. For $Co_{0.77}Rh_{0.23}$ these authors deduced for Rh a total magnetic moment of 0.62 μ_B. This is in reasonably good agreement with the data given in table 1.

Furthermore, the MCD-XA spectra recorded by Harp *et al* [5, 27], could be reproduced in a very satisfying way by making use of the scheme outlined in section 2 [28]. For this reason, one may also expect it to supply a sound and reliable basis for dealing with the MCD-XE spectra of ternary Co–Rh-based alloys.

From equation (4) it is quite obvious that the excitation step plays a crucial role for the MCD-XE spectra. To demonstrate this in some detail, theoretical spectra—broadened by Lorentzian and Gaussian profiles with widths of 0.5 and 0.15 eV, respectively—for $(Co_{0.85}Ni_{0.15})_{0.75}Rh_{0.25}$ are given in figure 3 for various photon energies $E_{in} = \hbar\omega_{in}$ of the excitation radiation. The top panel shows the polarization-averaged emission spectra $(I^+ + I^-)$ that obviously depend only moderately on the excitation energy. In particular, their structure hardly changes over E_{in}. Comparing these curves with figure 1 (top panel) one notes that they—as is to be expected—reflect the partial DOS of Rh rather directly. In contrast to $I^+ + I^-$, the dichroic signal $(I^+ - I^-)$ varies rapidly in amplitude as well as in sign if ω_{in} changes over a rather narrow range. On the other hand, if the excitation is done using radiation spread over a certain energy range ΔE_{in}, the changes for $I^+ - I^-$ are far less dramatic. As is shown in the lower part of figure 3 the shape of the MCD signal depends only slightly on ΔE_{in} and is shifted to higher values if ΔE_{in} is increased from 1 to 10 eV.

Accounting for the various broadening mechanisms in a realistic way, the theoretical spectra in figure 3 can be directly compared to corresponding experimental data. Within the experimental work on $(Co_{0.85}Ni_{0.15})_{0.75}Rh_{0.25}$ and $Co_{0.75}(Rh_{0.85}Pd_{0.15})_{0.25}$ mentioned above, *white light* over a range of about 140 eV has been used [9]. To account for this at least partly, the theoretical spectra that are compared in figure 4 with their experimental counterparts have been

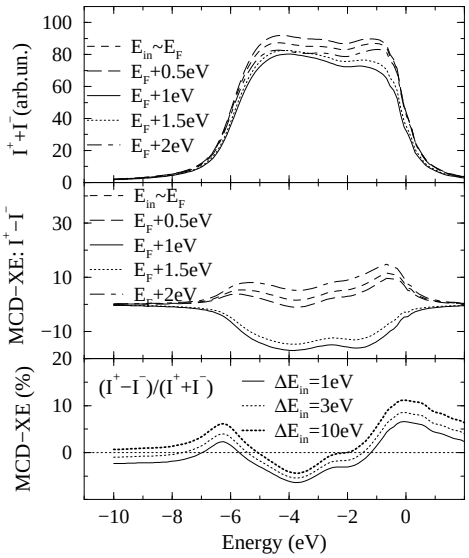

Figure 3. Theoretical XE (top) and MCD-XE (middle), $I^+ + I^-$ and $I^+ - I^-$, respectively, for $(Co_{0.85}Ni_{0.15})_{0.75}Rh_{0.25}$ for a specific photon energy for the excitation step, i.e. a specific initial-state energy E_i for the emission process. The panel at the bottom gives the relative MCD-XE spectra $(I^+ + I^-)/(I^+ - I^-)$ for excitation with photon energies spread over a range ΔE_{in}; i.e. the initial-state energies E_i lie between E_F and $E_F + \Delta E_i$.

obtained for $\Delta E_{in} = 10$ eV. For this comparison the theoretical spectra have been scaled down by a factor of about 10. There are several reasons for the experimental dichroic signal being much weaker than expected from theory. One is presumably the use of a rather wide range for the excitation energy. Even more important seems to be the fact that the measurements were done in an external field that was much too small to make the magnetization saturated [9].

The first set of theoretical spectra shown in figure 4 (dashed lines—broadening I) has been obtained using energy-independent broadening parameters. Comparing these with the corresponding spin-polarization curves in figure 2, one notes that the various curves go reasonably well in parallel with these. This finding is in accordance with the interpretation of the MCD-XE spectra already given by Strange *et al* [11] in the case of pure Fe. In figure 4 the experimental spectra reported by Gallet *et al* [9] have been added. When comparing with the above-mentioned theoretical spectra (labelled broadening I), one notes that the various features at higher binding energies are much more pronounced for the theoretical than for the experimental spectra. Using broadening parameters that increase quadratically with binding energy (broadening II in figure 4) a much better agreement with experiment is achieved. This clearly demonstrates that Auger relaxation processes within the valence band play a crucial role as regards the shape of the MCD-XE spectra, as was found before for conventional XES spectra [18].

4. Summary

Spin-polarized relativistic band-structure calculations have been performed for a number of Co–Rh-based disordered ternary alloys. Investigations of MCD-XE spectra of Rh revealed a strong dependency of these spectra on the excitation energy. This was found to be strongly reduced if a certain range of photon energies for the excitation step is assumed. Simulating the

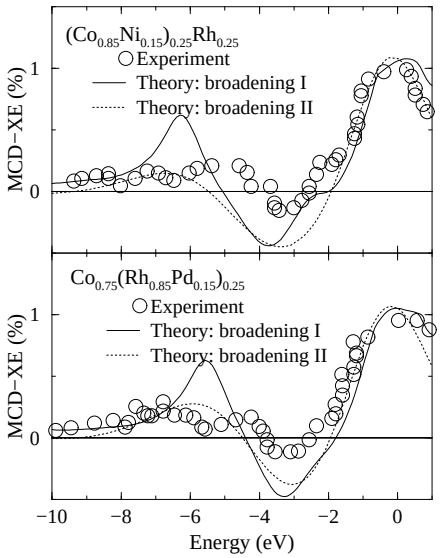

Figure 4. Theoretical and experimental MCD-XE spectra of $(Co_{0.85}Ni_{0.15})_{0.75}Rh_{0.25}$ and $Co_{0.75}(Rh_{0.85}Pd_{0.15})_{0.25}$. The experimental data stem from reference [9]. The theoretical spectra have been scaled down by a factor of about 10 (see the text). For the spectra labelled broadening I an energy-independent linewidth has been used. For spectra labelled broadening II it was assumed that the linewidth increases quadratically with binding energy.

experimental conditions accordingly, very satisfying agreement with recent experimental work could be achieved. As pointed out before by other authors, it was found that the interpretation of the MCD-XE spectra in terms of the corresponding spin polarization is quite well justified. However, there is no simple one-to-one relationship because the MCD-XE spectra are strongly influenced by energy-dependent broadening mechanisms.

Acknowledgments

This work was funded by the German Ministry for Education and Research (BMBF) under contract 05 621WMA 9 within the programme *Zirkular polarisierte Synchrotronstrahlung: Dichroismus, Magnetismus und Spinorientierung* and was done as a collaboration within the European TMR Network on *Ab-initio Calculations of Magnetic Properties of Surfaces, Interfaces and Multilayers*.

References

[1] Wienke R, Schütz G and Ebert H 1991 *J. Appl. Phys.* **69** 6147
[2] Thole B T, Carra P, Sette F and van der Laan G 1992 *Phys. Rev. Lett.* **68** 1943
[3] Schütz G, Knülle M and Ebert H 1993 *Phys. Scr.* T **49** 302
[4] Carra P, Thole B T, Altarelli M and Wang X 1993 *Phys. Rev. Lett.* **70** 694
[5] Harp G R, Parkin S S P, O'Brien W L and Tonner B P 1994 *J. Appl. Phys.* **76** 6471
[6] Kamp P *et al* 1999 *Phys. Rev.* B **59** 1105
[7] Tomaz M A *et al* 1998 *Phys. Rev.* B **58** 11 493
[8] Vogel J *et al* 1997 *J. Magn. Magn. Mater.* **165** 96
[9] Gallet J J *et al* 1998 *Phys. Rev.* B **57** 7835
[10] Akai H, Dederichs P H and Kanamori J 1988 *J. Physique* **49** 23

[11] Strange P, Durham P J and Györffy B L 1991 *Phys. Rev. Lett.* **67** 3590
[12] Weinberger P 1990 *Electron Scattering Theory for Ordered and Disordered Matter* (Oxford: Oxford University Press)
[13] Ebert H 1999 *Fully Relativistic Band Structure Calculations for Magnetic Solids—Formalism and Application (Springer Lecture Notes in Physics)* ed H Dreyssé (Berlin: Springer) to be published
[14] Rose M E 1961 *Relativistic Electron Theory* (New York: Wiley)
[15] Ebert H 1996 *Rep. Prog. Phys.* **59** 1665
[16] Hague C F *et al* 1993 *Phys. Rev.* B **48** 3560
[17] Müller J E, Jepsen O and Wilkins J W 1982 *Solid State Commun.* **42** 365
[18] Durham P J *et al* 1979 *J. Phys. F: Met. Phys.* **9** 1719
[19] Stepanyuk V S, Zeller R, Dederichs P H and Mertig I 1994 *Phys. Rev.* B **49** 5157
[20] Akai H *et al* 1984 *J. Magn. Magn. Mater.* **45** 291
[21] Ebert H, Zeller R, Drittler B and Dederichs P H 1990 *J. Appl. Phys.* **67** 4576
[22] Anisimov V I *et al* 1988 *Phys. Rev.* B **37** 5598
[23] Popescu V 1999 *PhD Thesis* University of Munich
[24] Williams A R, Moruzzi V L, Malozemoff A P and Terakura K 1983 *IEEE Trans. Magn.* **19** 1983
[25] Huhne T *et al* 1998 *Phys. Rev.* B **58** 10 236
[26] Ebert H and Battocletti M 1996 *Solid State Commun.* **98** 785
[27] Harp G R, Parkin S S P, O'Brien W L and Tonner B P 1995 *Phys. Rev.* B **51** 12 037
[28] Ebert H 1997 *J. Physique Coll.* **7** C2 161